

Particle Control in Phase Space by Global K-Means Clustering

J. Trier Frederiksen,¹ G. Lapenta,² and M. Pessah¹

¹⁾ Niels Bohr International Academy, Niels Bohr Institute, Blegdamsvej 17, 2100 København Ø, Denmark^{a)}

²⁾ Centre for mathematical Plasma Astrophysics, Department of Mathematics, KU Leuven, Celestijnenlaan 200B, 3001 Heverlee, Belgium

We devise and explore an iterative optimization procedure for controlling particle populations in particle-in-cell (PIC) codes via merging and splitting of computational macro-particles. Our approach, is to compute an optimal representation of the global particle phase space structure while decreasing or increasing the entire particle population, based on k-means clustering of the data. In essence the procedure amounts to merging or splitting particles by statistical means, throughout the entire simulation volume in question, while minimizing a 6-dimensional total distance measure to preserve the physics. Particle merging is by far the most demanding procedure when considering conservation laws of physics; it amounts to lossy compression of particle phase space data. We demonstrate that our k-means approach conserves energy and momentum to high accuracy, even for high compression ratios, $\mathcal{R} \approx 4$ — *i.e.*, $N_f \lesssim 0.25N_i$. Interestingly, we find that the most intuitive naïve approach to particle splitting does not yield accurate results over hundreds of simulation time steps. Rather, a more complex particle splitting procedure is superior. Implementation and testing is done using an electromagnetic PIC code, the Photon-Plasma code. Nonetheless, the k-means framework is general; it is not limited to Vlasov-Maxwell type PIC codes. We discuss advantages and drawbacks of this optimal phase space reconstruction.

Keywords: particle-in-cell codes, particle merging, plasmas, magnetic fields, k-means, vector compression

I. INTRODUCTION

Control of computational macro-particle (CMP) populations in Particle-In-Cell (PIC) codes is particularly desirable in at least two situations:

Population Runaway: Monte Carlo realizations of collisional processes in PIC codes, for example, often involves fractionation of CMPs into "parents" and "children" for enhanced statistical resolution of the collision processes. This results in explosion of CMP populations, and a memory bounded simulation longevity.

Load balancing: in PIC codes relies on the ability to redistribute CMPs among computational processes (e.g. in MPI domain decomposed models) at run-time to maintain similar execution times of the computational processes, and preserve statistical resolution of continuous phase space.

CMP de-population (re-population) of domains that are progressively filled (depleted) can be achieved through deletion (addition) of CMPs – for those domains which are oversampled (undersampled), while attempting to maintain physical quantities locally conserved. Single particle deletion (addition) CMPs is detrimental with respect to the conservation of the physical properties of the system being modeled^{5,9–11,16}. It is necessary to merge (split) several CMPs to conserve both momentum and energy from the phase space

information available.

An algorithm that can achieve this goal in a robust and efficient manner will benefit a wide range of problems in laboratory and astrophysical settings. Many physical processes naturally lead to runaway CMP populations (time domain), and extreme CMP concentrations (spatial domain), *e.g.*

Load: High-intensity laser-plasma wakefield acceleration of electrons, Beck¹ (also Figure 1).

Runaway: Gamma-Ray Burst wakefield plasma acceleration, under the influence of detailed Compton scattering, Frederiksen³.

Load: Streaming instabilities and agglomeration of planetesimals leading to planet formation, Johansen and Youdin⁷.

Runaway & load: High-energy radiative processes and pair cascades in pulsar magnetospheres, Timokhin and Arons²¹.

Load: Streams and caustics in the evolution of dark matter structures in cosmological simulations, Vogelsberger and White²².

All these cases (and many others) demand an efficient CMP population control and/or redistribution in large-scale numerical simulations.

Several strategies for CMP merging have been visited in the literature over the last few decades, changing in order of complexity, cost and accuracy. Lapenta and

^{a)}Electronic mail: trier@nbi.dk

Brackbill¹⁰, also later Lapenta⁹, considered the problem of merging/splitting on a single particle basis, e.g., $2 \leftrightarrow 1$, $3 \leftrightarrow 2$, and cell-based $N_{cell} \leftrightarrow M_{cell}$ approaches, (Lapenta and Brackbill¹¹), with N and M small. More recently, more complex algorithms have emerged such as agglomerate clustering⁵ and resampling, and also oct-tree reconstruction¹⁶ in momentum space.

Commonly, those previous strategies used means of algebraic reconstruction to ensure that physical field quantities, represented on the PIC discrete mesh (in \mathbf{r} -space) would be conserved exactly. Some were investigated in reduced-dimensional systems, e.g. 1D3V (Martin and Cambier¹⁶), although their method was not strictly constrained to 1D. Others further applied a reconstruction procedure which decomposed 6D phase space, $f(\mathbf{r}, \mathbf{p}, t)$, in to 3D subspaces, $f_r(\mathbf{r}, t)$ and $f_p(\mathbf{p}, t)$, employing strict algebraic reconstruction on \mathbf{r} -space, while retaining the solution found by agglomerate clustering in \mathbf{p} -space (Grasso et al.⁵). Any decomposition of phase space, \mathbb{R}^D , into phase subspaces \mathbb{R}^B and \mathbb{R}^C , with $B+C=D$ (for our case $D=6$), removes information contained in possible cross-correlation between the subspaces. It is conceivable that such correlations should be preserved.

In a view alternative to previous strategies, we consider the problem of reducing (increasing) particle phase space resolution by merging (splitting) CMPs, as an optimization problem in 6 dimensions. Our approach randomly selects existing particles as a global best guess at a solution for the clustering, with the objective to either merge or split them into a new imitative set of particles. Subsequently, a K-means iterative minimization of a global intra-cluster distance measure successively drives the merged (split) solution towards a reduced (increased) CMP population, with the same physical properties.

In Section II, we describe the natural relationship between k-means clustering and the PIC code phase space



FIG. 1. Early stage in ultra-high intensity laser pulse interacting with a quiescent homogenous plasma plume, showing electron CMP number density (colors not to scale). A bubble (dark central region), evacuated of electrons, is created by the highly non-linear disturbance from the laser field pulse (green, right), which is propagating to right. A hot-spot (yellow, left) in the wake of the laser pulls electrons along, at close to the speed of light. The highly inhomogeneous density, ranging from $N_{e,\min} \approx 1$ to $N_{e,\max} \approx 300$, severely affects load balancing. Our method can alleviate this problem to speed up the simulation by a significant factor.

representation. We then describe the details of our global k-means procedure; initialization, distance measure, particle merging and splitting, as well as an important edge-preserving measure to circumvent k-means artifacts on bounded domain decompositions. Section III outlines our test simulation setup and presents a few crucial tests of our k-means clustering procedure. Discussion and conclusions are given in Section IV.

II. K-MEANS CLUSTERING IN THE PIC CODES

Generally, in electromagnetic PIC codes, the source terms in Maxwell's equations, $\rho_c(\mathbf{r}, t)$ and $\mathbf{J}(\mathbf{r}, \mathbf{p}, t)$, are constructed from interpolated accumulation of a large number of computational macro-particles (CMPs) onto a computational mesh. These CMPs are distributed in *continuous* real space and momentum space, and given a continuous weight to signify the particle statistical influence. For very large numbers of CMPs, we can approximately describe the computational plasma everywhere by a distribution function, $f(\mathbf{r}, \mathbf{p}, t) \equiv \sum_s f_s(\mathbf{r}, \mathbf{p}, t)$, hereafter phase space density, where the subscript 's' denotes particle species.

In the Photon-Plasma code⁶, for the most complete case of 3D3V simulations, the CMP is represented by a six-tuplet of real numbers, $\tilde{\mathbf{r}} \equiv \{r_x, r_y, r_z, p_x, p_y, p_z\}$, which positions the particle in 6-dimensional phase space (the tilde signifies a 6D vector). Further each CMP is given a statistical weight, w_i , which dictates a relative strength of the particle with respect to either the number of physical particles, or a scaled amount of physical particles. Relativistic momentum is $\mathbf{p} \equiv m_0\gamma(v)\mathbf{v}$, with $\gamma \equiv \sqrt{1 - \beta^2}$, $\beta \equiv v/c$, and in the Photon-Plasma code we most naturally keep the CMPs' relativistic 3-velocity, \mathbf{p}/m_0 . For example $p_z = v_z(1 - \beta_z^2)^{-1/2}$ with $\beta_z \equiv v_z^2/c^2$. This renders direct addition and subtraction of particle momenta, vectorially, physically meaningful. Consequently, we may view the particle ensemble phase space as a collection of points in 6-dimensional Euclidean affine space, with a well defined algebra consisting of addition (e.g. $p_{z,i} + p_{z,j} = p_{z,k}$), subtraction (e.g. $x_i - x_j = x_k$) and a distance measure,

$$d^2(\tilde{\mathbf{r}}_i, \tilde{\mathbf{r}}_j) = (x_i - x_j)^2 + \dots + (p_{z,i} - p_{z,j})^2.$$

Particles can then be vectorially added or subtracted, and we can find a distance between them in this affine space. We can also construct an arithmetic mean, or for weighted particles, a weighted arithmetic mean of any ensemble, or cluster center point, of particles

$$\tilde{\bar{\mathbf{r}}} = \frac{\sum_i w_i \tilde{\mathbf{r}}_i}{\sum_i w_i} \Leftrightarrow \tilde{\bar{\mathbf{r}}} w_{cl} = \sum_i w_i \tilde{\mathbf{r}}_i, \quad w_{cl} \equiv \sum_i w_i, \quad (1)$$

where now barred vectors, i.e. $\tilde{\bar{\mathbf{r}}}$, denotes cluster points.

These simple facts form the basis of this paper and the justification of global k-means clustering as a way of optimal phase space reconstruction in, for example, PIC codes.

A. Weighted k-means clustering

Multivariate, multidimensional, data can be analyzed and manipulated using vector compression. K-Means¹⁴ belongs to this general class of vector compression algorithms, and can be used to either refine or coarsen multivariate data manifolds. The k-means objective is simple: from a set of M data points, $\{\tilde{\mathbf{r}}_1, \dots, \tilde{\mathbf{r}}_M\}$, with weights $\{w_1, \dots, w_M\}$, in D -dimensional space, \mathbb{R}^D , find K cluster centers, $\{\tilde{\mathbf{r}}_1, \dots, \tilde{\mathbf{r}}_K\}$, with weights w_1, \dots, w_K , also in \mathbb{R}^D , which partition the original data in the optimal way. This is defined as that partitioning which minimizes the total global intra-cluster distance,

$$\min(\tilde{\mathcal{D}}_{tot}) \equiv \min \left(\sum_{j=1}^k \sum_{\tilde{\mathbf{r}}_i \in \tilde{\mathbf{r}}_j} \|w_i \tilde{\mathbf{r}}_i - w_{cl,j} \tilde{\mathbf{r}}_j\|^2 \right), \quad (2)$$

with $\tilde{\mathbf{r}}_j$ and $w_{cl,j}$ defined as the j 'th cluster center and j 'th cluster weight by equation 1 (left), respectively (right).

We choose to work in this paper in normalized data space, such that $\{r_x, \dots, p_z\} \rightarrow \{r_x/L_x, \dots, p_z/L_{pz}\}$, where $\{L_x, \dots, L_{pz}\} \equiv \{\max(r_x) - \min(r_x), \dots, \max(p_z) - \min(p_z)\}$; this choice is specific to our problem, since we cannot *a priori* assume that certain directions in phase space are more important than others with respect to the physics, if we want the procedure to be generally applicable and fast.

In signal compression theory, the original data set to be compressed or inflated in k-means is often denoted 'training vectors' while the solution (the clustered data set) is called the 'codebook vectors'. We adopt this terminology henceforth.

1. Computational Effort of K-means

Finding the *global* minimum for any data set in higher dimensions in k-means is an NP-hard task. For given values of M , K and D , the computational effort is approximately $\mathcal{O}(M^{KD+1} \log M)$ which is intractable for almost any PIC code problem we want to consider. If we — on the other hand — accept the solution to be only approximative we can find acceptable alternatives in finite time, and even quite fast. Equivalently, an approximate solution amounts to a *local* minimum rather than the global minimum described by Equation 2).

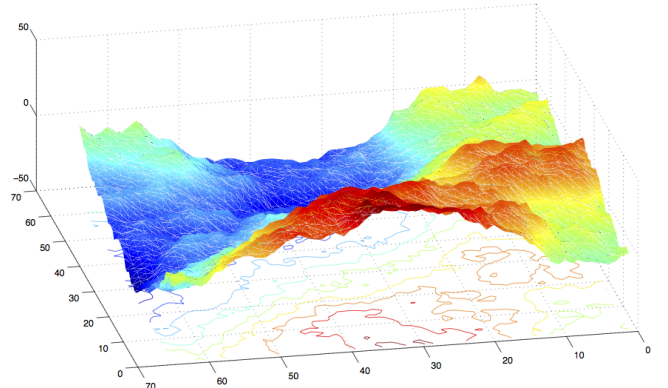


FIG. 2. Illustration: finding the global minimum in k-means is NP-hard for $D \geq 2$ dimensions and $K \geq 2$. However, for approximate solutions, i.e. when finding only a *sufficiently* global minimum, heuristic algorithms converge quickly. Arbitrary data set generated in MATLAB⁸.

2. K-Means Clustering, Lloyd-Forgy algorithm

A variety of heuristic algorithms exist; commonly they use iterative processes to find a local minimum solution to Equation 2. The simplest brute force heuristic algorithm, which is also the most expensive, is Lloyd's algorithm¹⁷ Lloyd¹³ with Forgy initial conditions Forgy². We will use "Lloyd's" algorithm and "k-means" interchangeably, even though the "k-means" term and a more general treatment of vector quantization originates from MacQueen¹⁴. Lloyd-Forgy, or k-means clustering optimization goes through three basic steps:

- 1. Initial condition:** a first guess as to a solution is made by placing the initial codebook vector set. Forgy's method at random selects K training vectors as the initial codebook. This often (but not always) is better than for example choosing random points within the data space.
- 2. Cluster assignment:** training vectors are assigned each to their nearest codebook vector (cluster center). This is effectively a Voronoi tessellation step.
- 3. codebook replacement:** by calculating the weighted arithmetic mean (Equation 1), based on within-cluster associated training vectors, new codebook centers are found to replace those codebook vectors found in 2) during the previous iteration.

Steps 2 and 3 are repeated until some defined convergence threshold is met; for example, as in this paper, when the ratio in total error (eqn. 2) between successive iterations changes by less than 1% is a common criterion¹⁸. Figure 4 illustrates the algorithm for a two-dimensional case.

The effect of successively tessellating and cluster recentering, respectively, reduces the computational effort

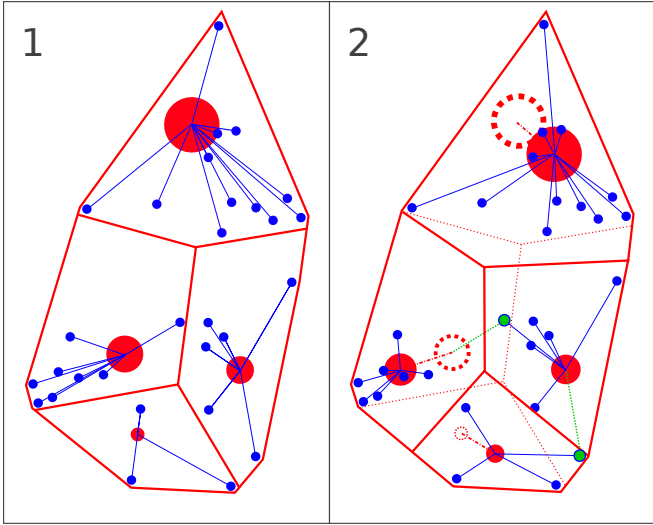


FIG. 3. Weighted Lloyd-Forgy iterative clustering ("k-means") in 2D. *Panel 1*: initialize codebook (red disks) at randomly chosen training vectors (blue dots), and perform Voronoi tesselation. *Panel 2*: compute new weighted arithmetic means of training vectors within each Voronoi cell and re-define these means as the codebook vectors. Adjust weights. NB: some training vectors will migrate to other cells (green dots). Dashed lines represent previous iteration; Voronoi cell boundaries (red lines), cluster positions (red open circles) and migrated training vectors (green lines). Reiteration is performed until a convergence criterion is met.

to $\mathcal{O}(M \times K \times D \times i)$, with i the number of iterations to convergence. Nonetheless, even when employing Lloyd-Forgy, the computational expense becomes increasingly prohibitive for large values of M , K and D . Hence, we might expect to discard k-means as feasible for CMP merging/splitting in PIC codes, especially for global or semi-global simulation volumes. In this paper we demonstrate its feasibility in terms of *physics*, rather than consider computational costs. Elsewhere (Malý et al.¹⁵) it is reported that by employing various accelerated partitioning and distance calculations, or employing brute force GPGPU kernels, the running time is reduced to acceptable levels, thus demonstrating its feasibility in terms of *computation* as well.

3. Contractive artifacts of K-Means

The convex hull of a k-means solution will always *contract* with respect to the original data set volume, i.e.

$$\int_{\Omega} d\Omega f(\tilde{\mathbf{r}}, t) < \int_{\Omega'} d\Omega' f'(\tilde{\mathbf{r}}, t) ,$$

except for the trivial case ($f' == f$). Here $\Omega, \Omega' \in \mathbb{R}^D$ are the convex hull bounding surfaces of the CMP density distribution in D dimensions before and after k-means compression. We have sketched this — for PIC

code applications undesirable property of k-means — in Figure 4 for $D=2$.

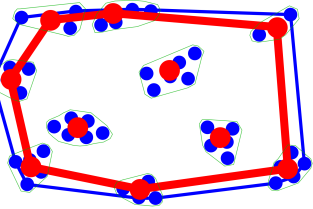


FIG. 4. Phase space volume contraction associated with k-means clustering in 2D. The convex portion of phase space (red perimeter line) spanned by the codebook clusters (red dots) will always be smaller than portion of phase space (blue perimeter line) spanned by the training vectors (blue dots). This effect is undesirable effect as it leads to edge depletion effects for $\rho_c(\mathbf{r})$ and $\mathbf{J}(\mathbf{r}, \mathbf{p})$.

For PIC codes which are parallelized over computational processes via domain decomposition in real space ($\mathbf{r} = \{r_x, r_y, r_z\}$) this is problematic because a given volume will experience edge artifacts in charge density, $\rho_c(\mathbf{r})$, and current density, $\mathbf{J}(\mathbf{r})$, namely a reduction of particles' contribution to those physical quantities. Domain decomposition is often employed in PIC codes, making such an edge-preserving step indispensable.

To alleviate this problem we devise a simple "quick-and-dirty" edge-preserving correction scheme, which is illustrated in Figure 5. The idea is simply to let the clustered codebook solution approach the original training vector set on the domain boundaries. The boundary thickness is presently defined as equal to two cells of width. In this way we ensure that edges are left untouched. In terms of computation, this leads to an extra iteration which we estimate at effort $\mathcal{O}(M \times K)$, thus not severe (yet not ignorable) in the total budget. Furthermore, the final number of codebook vectors will be slightly larger than the target value for large volumes and approach the original number of training vectors when the volume in question approaches PIC code cell size.

This mock edge-preserving procedure is simple; after having found a codebook solution on the entire domain (including the boundary region), the codebook vectors in the domain boundary are deleted, and the training vectors kept here instead. On the interior of the domain (excluding boundaries), the codebook is reduced if the cluster falls inside but has training vector members in the domain boundary. If a codebook vector resides on the interior and has *all* training vector members on the interior as well, the codebook is kept as-is and the training vector members are deleted.

In Section III we demonstrate that, despite its simplicity this edge-preserving scheme manages to suppress significantly and adequately the edge-effects introduced by the contractive artifacts of k-means clustering, as should be appreciated from Figure 12.

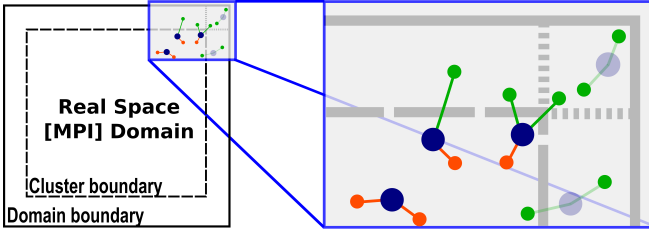


FIG. 5. Our "quick-and-dirty" edge-preserving procedure, for spatially domain decomposed simulations. The procedure is applied only in those dimensions, where the convexity of the k-means leads to systematic edge effects. Shown in the inset on the right are: kept/omitted codebook vectors in dark blue/light blue, kept/deleted training vectors in green/red. See main text for further explanation.

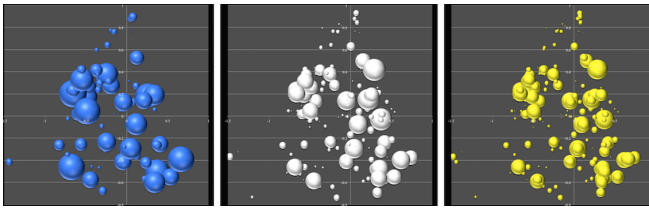


FIG. 6. Illustration of compressing / inflating a PIC code particle data set, using k-means clustering. *Middle*: the original 6D phase space data set (144 particles) projected into 2D momentum subspace, P_x - P_y . *Right*: an inflated set of 216 particles, optimally resembling the original data set, effectively increasing phase space resolution by many-to-many particle "splitting". *Left*: a new set of only 72 particles, optimally representing the original data set, effectively a many-to-many merge. NB: weights (sphere radii) are only approximately to scale.

4. Particle Merging — Employing K-Means

From the previous section, merging particles many-to-many, globally (or semi-globally) in the volume now becomes obvious; after the k-means operation, the codebook will contain all the necessary phase space information needed to preserve the physics in the continued simulation.

We need only delete the original particle data (the training vectors) and replace them with the new reduced particle data set (the codebook)

$$\{\tilde{r}_1, \dots, \tilde{r}_M\}_{\{s, tr\}} \rightarrow \{\tilde{r}_1, \dots, \tilde{r}_K\}_{\{s, cb\}},$$

while conserving total charge, globally, by preserving the total weight of the CMPs, pre- and post-compression:

$$\sum_j^K w_{cb} = \sum_i^M w_{tr}, \quad (3)$$

One further constraint is

$$w_{cb} = \sum_l^{N_{cl}} w_{tr,l}, \quad (4)$$

for all N_{cl} intra-cluster particles. Here 'cb' ('tr') denoting codebook (training) vectors, respectively, and 's' denoting species.

Several schemes exploit the additive properties of phase space, and they can be classified according to the approaches mentioned in the Introduction. The advantage of a many-to-many ($M \rightarrow K$, $M, K \gg 1$) iterative optimizing approach, like ours, is that we do not have to consider specifically, nor analytically, conservation of physical properties, e.g. energy, momentum, space charge density, current density or any higher order moments of the distribution.

The many degrees of freedom ensures total conservation of the physics to any desired precision¹⁹. The quality of the iterative solution will however be practically constrained by computational expense, and by demands on the number of particles (needed to resolve the physics) in the simulation.

5. Particle splitting, a symmetry argument

An accurate method for splitting particles is also needed; when the particle number in a cell falls below some given threshold, an increase in phase space resolution becomes imperative — even for physical reasons. Simply on-top splitting into many new particles^{5,10} is fast, and seemingly precise at the time of splitting. However, it turns out that the simple on-top split may not necessarily be the best choice. We will demonstrate this in a stress test of particle splitting procedures (Section III).

Counter-intuitively, we choose to exploit a symmetry of the k-means procedure. Increasing statistical resolution by adding particles can be achieved as accurately as merging by *keeping* all training vectors, and *adding* the codebook vectors

$$\{\tilde{r}_1, \dots, \tilde{r}_M\}_{\{s, tr\}} \rightarrow \{\tilde{r}_1, \dots, \tilde{r}_M\}_{\{s, tr\}} + \{\tilde{r}_1, \dots, \tilde{r}_K\}_{\{s, cb\}}.$$

Effectively, all new particles (codebook vectors), are placed *precisely* on the 6D phase space manifold, but at positions *different* from those of the original particles (training vectors), in 6D phase space. This amounts to a k-means phase space *inflation* of type $M \rightarrow K \Rightarrow M+K$, in terms of number of CMPs. A split which could have been simply $\mathcal{O}(K)$, now becomes a rather expensive — as expensive as k-means for merging — $\mathcal{O}(M \times K \times D \times i)$ once again. Why do this?

The only difference from merging is that we need to redistribute the total weight of the original particle data,

on *both* training vectors and codebook vectors

$$\sum_j^K w_{cb} + \sum_i^M w_{tr} = \sum_i^M w'_{tr},$$

where now the ' (prime) denotes values before performing k-means. Practically, the re-distribution of weights in our k-means based splitting scheme is done by sharing the weights between training vectors and their associated codebook vector in proportion to the training vectors' weights. The total amount of weight, w_{cb} , given to a codebook (cluster center), is the average value of those intra-cluster training vectors,

$$w_{cb} \equiv \langle w_{cl} \rangle \frac{w_l}{w_{cb}}, \quad \langle w_{cl} \rangle \equiv \frac{w_{cl}}{N_{cl}}$$

is the mean weight in that cluster, and

$$w_{cl} \equiv \sum_l^{N_{cl}} w_l,$$

and w_l are the individual weights of the N_{cl} training vectors in that cluster. This is done under constraints of the edge-preserving scheme described above (Section II A 3).

When taking into account an accelerated k-means algorithm (Malý et al.¹⁵), the computational cost issue is relaxed, and we can afford the extra care taken in *oversampling* phase space for increased statistical resolution.

III. PROOF OF CONCEPT: 'BARBARA' TESTS

We proceed to demonstrate k-means based merging/splitting feasibility in terms of preservation of physics with heavily varying particle numbers.

All tests in the remainder of this article have been performed using a slightly modified setup of a simple 2D3V relativistic two-stream simulation, used for tests of the **Photon-Plasma** code⁶. A relativistic neutral electron-ion beam is streaming through a neutral electron-ion background at $\Gamma_{beam} = 3$, with density ratio $n_b/n_{bg} = 1/3$. The dynamics are thought to be of relevance in cases such as Gamma-Ray-Burst afterglow shocks in a circumburst medium⁴.

Our reference 'barbara' case in the present paper has grid size $N_{x,z} = 128$, $N_y = 1$, physical size $L_{x,z} = 12\delta_e = 3\delta_i$, $L_y = 1.2\delta_e = 0.3\delta_i$, $m_i/m_e = 16$, beam Lorentz factor $\Gamma_b = 3$, beam-to-background density $n_p/n_b = 1/3$, $\omega_{pe,0} \approx 12$, $\delta_e = 0.0856$, so $\delta_e/\Delta_x \approx 8.6$. Time step $\Delta t = 0.00391$, $t_{end} = 10.0 \approx 120\omega_{pe}^{-1} \approx 30\omega_{pi}^{-1}$, $N_p = 30$ in the background and $N_b = 10$ in the beam plasma per cell/species; a total of 80 particles/cell.

The detailed reference simulation setup is not important for our tests; the only objective is to see how well we preserve the physics w.r.t. a reference case. Throughout this Section, the 'reference run' denotes the instance of 'barbara' which is devoid of performing merging and splitting.

Although our simulations are setup in a quasi-2D3V reduced dimensionality, but this does not influence our k-means tests, since particles still have a single cell's degree of freedom, even in the Y -coordinate. When we take into account the normalization of data space (see Section II A), we will have a truly 3D3V phase space manifold to work with.

The simulations were all done on a 4x4 MPI domain decomposed geometry, using simply the MPI processes as our k-means domains. Still, domain sizes are not limited in any way, except for a lower bound on volume of a few cells in each spatial dimension. This is because the edge-preserving scheme will make the solution approach the original phase space density for very small volumes of order *a few* cells, $V_{kmeans} \equiv k\Delta_x l \Delta_y m \Delta_z$, where $\{k, l, m\} \rightarrow \{1, 1, 1\}$.

We have verified the binary authenticity of successive reference runs, and that runs of 'barbara', using actual merging/splitting, were also binarily identical to the reference run – up to the point of first k-means, of course.

A. Pure particle merging & splitting stress test

A severe stress test was performed to ascertain the quality and longevity of clustered solutions under what we defined as 'extreme' conditions.

Multiple merges (or splits), only, were performed successively until the solution were no longer meaningful when comparing with the (constant particle number) reference run. After running the simulation for about 400 iterations ($33\omega_{pe}^{-1}$), we either only merged or only split the total particle number four times over the course of an additional 260 iterations ($22\omega_{pe}^{-1}$).

The merging stress test successively removed 2/3 of the former number of particles, for all species, on all MPI processes. Thus, from the first merge to the last merge, the number of particles would be $N_f/N_i = (1/3)^4 \approx 0.01$, had the fraction been exactly $1/3$. However, since we employed the mock edge-preserving scheme (see Section II A 3) included which limits the boundaries to the true solution CMP number density, the remaining particle number fraction in each merging step was somewhat higher than $1/3$. In fact the final-to-initial CMP total particle number was rather $N_f/N_i \approx 0.1$.

In a similar fashion, we conducted a splitting test, which of course is less severe, which successively added 1/3 of the former number of particles, for all species, on all MPI processes, to the new solution. We emphasize our use of the expensive on-manifold k-means based splitting (see Section II A 5); the cheap on-top split yielded meaningless results — see also Section III A 1. Now, instead, the number of particles would have increased to $N_f/N_i = (4/3)^4 \approx 3.2$, had the added fraction been exactly $1/3^{rd}$. Again, the mock edge-preserving scheme limited the true solution total number of CMPs to $N_f/N_i \approx 2.8$.

The resulting evolution of the merged and split cases

are worth comparing for a quantity which is solved for by *integration*, rather than comparing Maxwell's source terms, \mathbf{J} and ρ_c , formed by the particle data, directly. In Figure 7 and Figure 8 we compare $B_y(x, z)$ for splitting (left panel), reference (middle panel) and merging (right panel) cases, for two splits (or merges) over 65 iterations, and four splits (or merges) over 260 iterations, respectively. In the latter case, the last merge was done 100 iterations prior to the snapshot shown in the figure. All three panels are contoured on the same color scale, in each of the figures separately; they are directly comparable.

Not surprisingly, the splitting produces a perfect match with respect to the reference case, for all cases. Everything is preserved at close to machine precision. Also as expected, the merged simulation shows increased levels of Poisson noise in the field as the number of CMPs is reduced. Still, after having removed more than 75% of the original data set, and after several tens of iterations, the solution is still very good. Even after having removed more than 90% of the particles over an additional 200 iterations, although the noise levels have risen considerably the overall. The global evolution is well preserved. Although high-k noise has been introduced, the total energy and momentum are conserved to better than $\sim 0.1\%$ and the global field structure is intact. We have checked the Fourier spectra which show this behavior as well; high-k modes are rising during a merge stage, but the spectrum remains largely unaltered for low- and intermediate-k wavenumbers.

This stress test sets limits on the severity of compression parameters and resilience of compressed solutions. Much like image compression, we see that a reduction works well even for very high compression ratios, like for example compressing bitmapped images (.bmp) to Joint Photographic Experts Group images (.jpg), although the compression algorithms for images are likely more sophisticated in the latter case.

A first, back-of-the-envelope quantification of validity of compression solutions hints that we should not com-

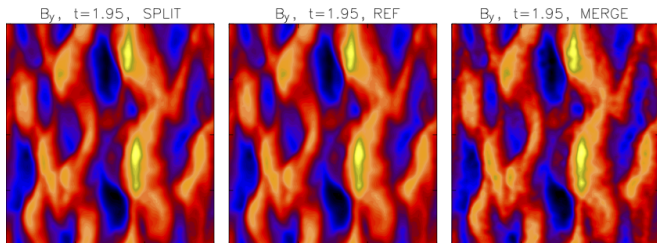


FIG. 7. Comparison of $B_y(x, z)$ for a hard stress test of merge (right panel) and split (left panel) with the reference case (middle panel), at time $t \sim 23\omega_{pe}^{-1}$. The number of particles has been merged (split) twice, into $N_f/N_i \approx 4/17$ ($N_f/N_i \approx 32/19$). The simulation subsequently ran for 65 iterations. Total energy and momentum conservation is better than $\sim 0.01\%$.

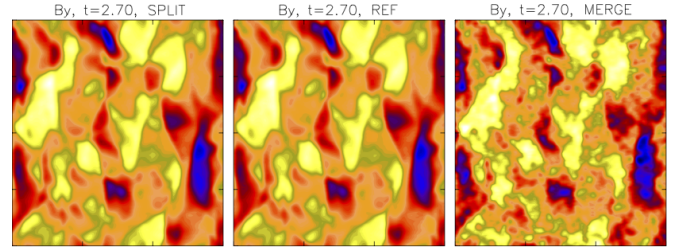


FIG. 8. Same as Figure 7, but now, at time $t \sim 32\omega_{pe}^{-1}$. The total number of particles has been merged (split) into $3/32$ ($31/11$) in four steps over the course of 260 iterations. The stress test has severely increased noise. Global field structure and power is unaffected. Energy and momentum is still conserved to about $\sim 0.1\%$, despite the noise introduced by reduced statistics.

press (merge) successively more than 2 or 3 times without replenishing the CMP ensemble (either by advection or by production through collisions or simple statistical splitting). Furthermore, the compression ratio should not exceed about $\mathcal{R}_{merge} \equiv N_f/N_i \approx 2/3$ and not be performed successively within less than about a plasma-oscillation (10-20 iterations here). This estimate is based on empirical evaluation, and is definitely subject to refined studies and analysis.

1. *Naïve versus k-means splitting test*

More surprisingly, however, comparing the expensive k-means splitting procedure with naïve on-top splitting (copy particles, $\tilde{\mathbf{r}}'_i \equiv \tilde{\mathbf{r}}_i$ and sharing weights, $w'_i + w_i \equiv w_i$), we find that the solutions are nowhere near to being similar. A fraction of the particles for all three cases are plotted in real subspace, $\tilde{\mathbf{r}}_{2D} = \{x, z\}$ for on-top split (left panel), reference (middle panel) and k-means on-manifold splitting (right panel), in Figure 9. The k-means on-manifold split solution traces the reference solution extremely well, while the on-top split does not even begin to compare with reference, the solution is gone.

A plot of *differences* in position on the phase position subspace manifold, $\tilde{\mathbf{r}}_{1D1V} = \{z, p_z\}$, for three different times, $\Delta t \approx 0.17\omega_{pe}^{-1}$, $\Delta t \approx 1.0\omega_{pe}^{-1}$, $\Delta t \approx 1.83\omega_{pe}^{-1}$ — proceeding a single split (no other influence) — reveals a strong growth in dissimilarity for the on-top naïve split. This behavior we did not observe for the on-manifold (expensive) k-means split described in section II A 5. On a note: the discrepancy seems to be bigger, perhaps even to emanate from, the forefront of the phase space waves (middle panel) of the streaming instability. Thus we could speculate as to a physical artifact of a PIC code formulation origin of this in the on-top splitting method.

To test this in the extreme limit of many iterations post-split, we ran the single split test for a total of 200 iterations in both the on-top and on-manifold splitting cases, and then looked at the difference with respect to

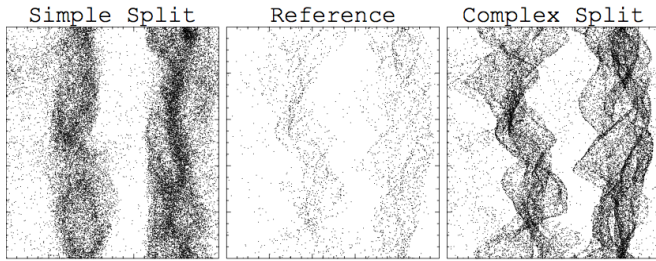


FIG. 9. 4% of the beam electrons (barbara species 3) plotted immediately following the last of eight splits – $t=3.910$, $N_f/N_i = 7.82$ – as function of position in $\{x, z\}$ phase subspace. The complex split procedure makes the phase space inflation follow the reference phase space manifold almost exactly. The simple split solution is meaningless at this stage.

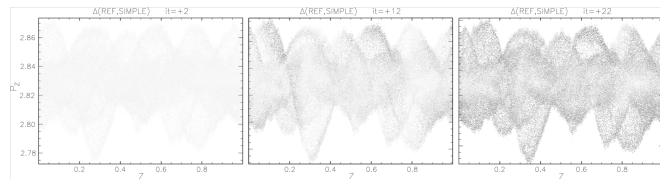


FIG. 10. Deterioration of simple split solution w.r.t. time. After +20 iterations from split, the solution is significantly altered. The difference between all particles in the reference run and the simple one-split only run has been taken in $\{z, p_z\}$ phase subspace

the reference case. The result is given in Figure 10, where it is clearly seen that the on-top split produces a solution which deviates not only significantly, but even so detrimentally, from the reference — the on-manifold split exhibits no appreciable dissimilarities, yielding an almost flat field.

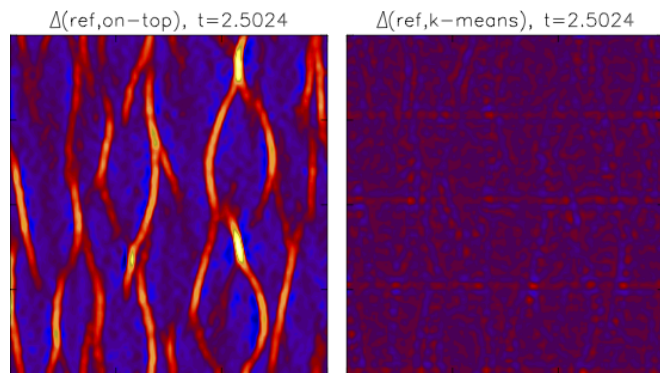


FIG. 11. Differences between a single on-top (left) and on-manifold split (right) with respect to reference, plotted in $\rho_c\{x, z\}$ subspace for beam ions. The on-manifold k-means split is superior, being almost a flatfield. The horizontal lines seen in the right panel are absent when we employ our edge-preserving scheme (section III B). The number of iterations, post-split here is 200.

While it may seem most natural to use a cheap and straightforward 'copy-on-top' (copy particles, $\tilde{r}'_i \equiv \tilde{r}_i$ and sharing weights, $w'_i + w_i \equiv w_i$) splitting method, this will *not* generally yield acceptable results. Counter-intuitively, rather, an expensive k-means based split – as described in Section II A 5 — will produce a significantly more correct solution, when integrated over several time steps.

B. Edge-preserving mock scheme tests

As previously explained, the k-means procedure possesses an intrinsic and undesired property when it comes to preserving the physics in PIC simulations. Since any calculation exploiting arithmetic means will produce volumes smaller than the original one, a domain decomposed PIC simulation will suffer boundary effects in the domain decomposition dimensions. For our case of the **Photon-Plasma** code, this is in phase subspace $\tilde{r}_{3D} = \{x, y, z\}$ (see also Section II A 3). In fact, it will even suffer this constraint in the domain *non*-decomposed dimensions (here momentum phase subspace, $\tilde{r}_{3V} = \{p_x, p_y, p_z\}$).

The 3D boundaries completely predictable, and it makes sense to counter-balance convexity issues of the k-means based procedure based on a spatial filtering of the real space coordinate boundaries. We regard $\tilde{r}_{3D} = \{x, y, z\}$ as correctable. Momentum subspace boundaries, $\tilde{r}_{3V} = \{p_x, p_y, p_z\}$, are regarded as non-correctable since in any trivial – they will generally not be regular. This is clearly depicted in Figure 10, where the boundaries in the z -direction are very regular. In the p_z -direction, however, things are not so predictable. We stress that we have *not* decoupled 6D phase space reconstruction by this procedure, only, we have ensured the convergence of the compressed (or inflated) k-means solution in a subset of dimensions. We have introduced no decoherence between position and momentum at all by this edge-preserving correction.

Two tests were performed to check the mock edge-preserving scheme performance

Thermal cases: with little or no bulk flow which leads to little or no replenishment of domain boundaries, keeping the domain boundaries quasi-static in terms of phase space evolution.

Streaming cases: the well evolved two-stream simulations would produce extreme replenishment of domain boundaries which will test the scheme's ability to render advection across boundaries transparent.

These two extreme dynamics are often realized in PIC codes, even simultaneously.

The test results from the thermal case are shown in Figure 12. We performed a single merge (split) — and

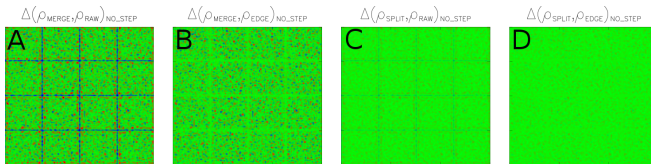


FIG. 12. Test of the mock-up edge preserving procedure. (A) (B): a single merge is performed with the usual PIC integration cycle completely omitted; the pure effect of the merge scheme is captured. Panel A(B) shows the merge without(with) edge-preservation effort, respectively. (C) and (D): same, but now a single SPLIT is performed instead.

nothing else — using the 'raw' non-corrected k-means algorithm, and a single merge (split) with our mock edge-preserving correction added to the k-means solver. The MPI domain boundaries are clearly visible. As expected the effect is more severe in the merging case since a split retains clusters with in-boundary particles whereas merging removes them. Still, even for merging, our edge-preserving correction yields significantly improved conservation properties. In both cases, not surprisingly, splitting was almost perfect. Particle merging naturally showed a minor decay in the solution across the merge step since it is a case of lossy compression. Still, the edge-preserving scheme forces the correct solution when approaching the real phase subspace boundaries, i.e. $f'(x, y, z) \rightarrow f(x, y, z)$ for $\{x, y, z\} \rightarrow \{x, y, z\}_{\min, \max}$. The solution following several integrations would not decay rapidly. This result was reinforced by the streaming test case showing no appreciable discontinuities and ability to smooth away the boundary 'shadows' introduced by the contractive aspect of k-means arithmetic averaging.

C. Full scale automated merge/split test

We conducted two tests with the full scale automated MPI-domain based merging-splitting activated: a "wide" and "narrow" tolerance range test would decide how well, and how often splitting and merging should be employed.

"Wide": tolerance yielded splitting when, for any MPI domain, $N_p < N_{low} \equiv 0.667N_{opt}$ and merging when $N_p > N_{high} \equiv 1.333N_{opt}$

"Narrow": tolerance yielded splitting when, for any MPI domain, $N_p < N_{low} \equiv 0.9N_{opt}$ and merging when $N_p > N_{high} \equiv 1.1N_{opt}$.

Due to the more restricted tolerance, the "narrow" test case yielded about twice as many splits and merges during the entire simulation, therefore also twice as many passes through the domain boundary edge-filtering. We have plotted the differences w.r.t. reference when running raw, respectively edge-preserving, k-means in Figure 13, for the "narrow" (panels 'A'=raw and 'B'=edge-

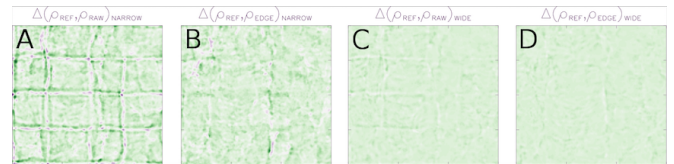


FIG. 13. Test of automatic merging and splitting. (A) and (B): procedure employing narrow tolerance range for the cases of "raw" and "edge-preserving" cases, respectively. (C) and (D): procedure employing wide tolerance range for the cases of "raw" and "edge-preserving" cases, respectively. The mock edge-preserving method is clearly superior.

preserving) respectively "wide" (panels 'C'=raw and 'D'=edge-preserving) tests. The effect of the more frequent splits/merges for the "narrow" case shows that traces of the MPI boundaries are visible in both the raw and edge-preserving cases, albeit the quality of the edge-preserving scheme still is superior by about a factor of ~ 5 -10.

For the "wide" tolerance case, the infrequent need for splits/merges both show improvement in handling the domain boundaries, again the edge-preserving scheme is justified by a factor 5-10 improvement. For the remainder we will concentrate on the "wide" tolerance case. More than 900 iterations, 100 merges, and 100 splits, were performed (6 splits and 6 merges for each MPI domain). The splitting/merging kicks in at approximately the end of linear instability growth; this is expected since growth of current filaments, and charge separation results in concentrations of computational particles at that approximate time.

Energy conservation

We stated earlier that total energy conservation and momentum conservation is remarkable, when we simultaneously take into account the preservation of structures — both spectral and spatial. In Figure 14 is plotted the difference, $\Delta E(\text{ref,edge}) \equiv E_{\text{ref}}(t) - E_{\text{edge}}(t)$, $\Delta E(\text{ref,raw})$, in total electromagnetic field energy, and the *negative* difference, $\Delta E(\text{edge,ref})$, in total particle energy, between the reference and "wide" test cases. Although the drift in EM energy is relatively large over time (about $1 \cdot 10^{-4}/2 \cdot 10^{-3} \sim 0.05 = 5.0\%$), this energy drift is compensated by an anti-correlated drift in the total particle energy (see Figure 14). This particle energy drift is partially due to the convex artifacts of k-means, operating in momentum space — which leads to a small artificial cooling. For a single split or merge, energy and momentum is conserved almost to machine precision. The total energy deviates less than 0.5% from reference in the case of wide tolerance range at the end of the simulation, after more than 200 merges and splits over more than 2000 iterations.

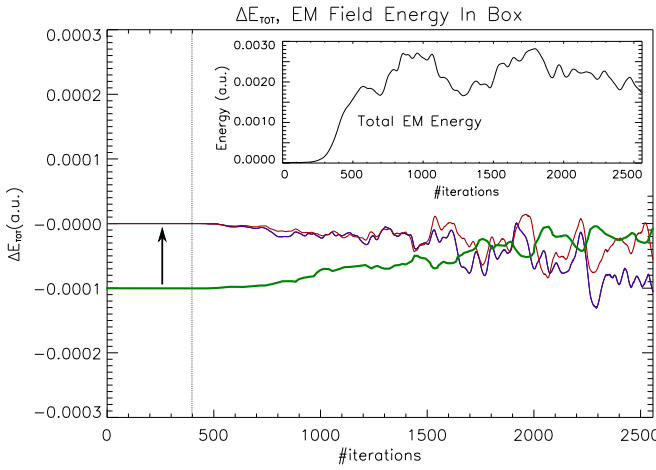


FIG. 14. Drifts in electromagnetic field energy (blue and red) and total negative particle energy (green, offset by -0.0001 for clarity) in the "wide" automated test case, using either a "raw" (blue) or an "edge-preserving" (red) methods (see section II A 3 on edge preserving mock-up procedure). Inset: total EM energy in the simulation volume as function of iterations.

Momentum conservation

Likewise, we can study the total momentum evolution, but it would yield little new information since the total momentum is still conserved to about machine precision (or at least k-means tolerance levels). Rather, it would make sense to look at a "critical" component of the momentum; the ion beam momentum in the streaming direction. We have plotted the time evolution for this quantity in Figure 15. It is unnecessary to plot any other histograms in phase subspace since all directions are equally valuable in the k-means optimization procedure; they will show comparative accuracy. There is a slight shift of the k-means treated runs (red curve) in the histograms as time progresses. We interpret this in connection with the conclusions concerning energy as a loss of energy transfer between particles and fields, which leads to a slower slow-down of the ion beam.

Particle weight distribution evolution

Figure 16 plots the evolution of particle weights (all particles) as the simulation progresses. From an initial constant weight, $w_{init} = 0.3$, weights become distributed in a uniform manner over a wide range of values, as new generations of particles appear due to merging and splitting. This is desirable in terms of statistical evolution; phase space information is now spread over a wide range in weights, and not only in phase space position. We can more safely destroy particles at random without risking serious biasing effects on the physics in the process.

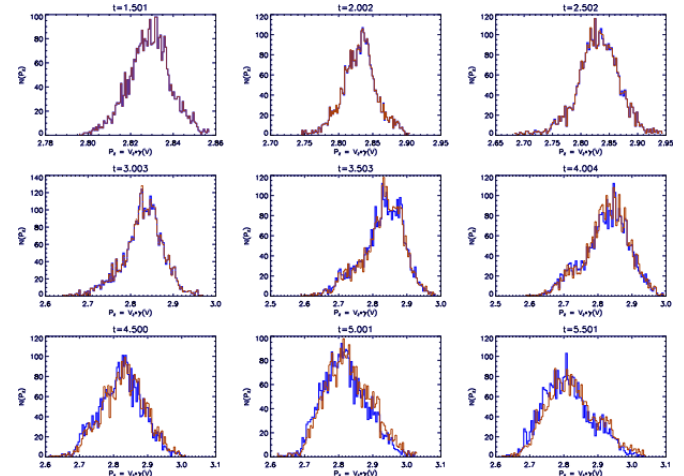


FIG. 15. Sample histogram of momentum space, ion beam species, along streaming direction, $\{P_z, N_p(P_z)\}$, for various times from just prior (upper left panel) to first merge, until about 1100 iterations ($\sim 48\omega_{pe}^{-1}$) later.

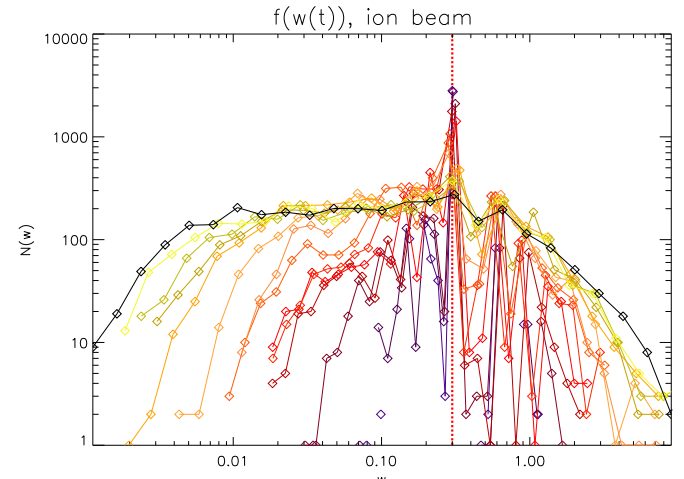


FIG. 16. Time evolution of particle weights, ion beam. Red dashes show the initial weight of all particles. Black curve final weights distribution at $t=10.0$ (#it = 2553). Dark-to-light colored curves correspond to early-to-late time distributions, over time intervals of 128 iterations.

Figure 18 compares the beam ion density at the very last time step, after 2553 iterations and more than 100 splits and 100 merges. The result demonstrates that the solution stays stable for rather long times. There is a tendency for the particles to clump due to the frequent merges; the edge-preserving performs slightly better in avoiding clumps, and better preserves large scale structure and flow — by a marginal measure.

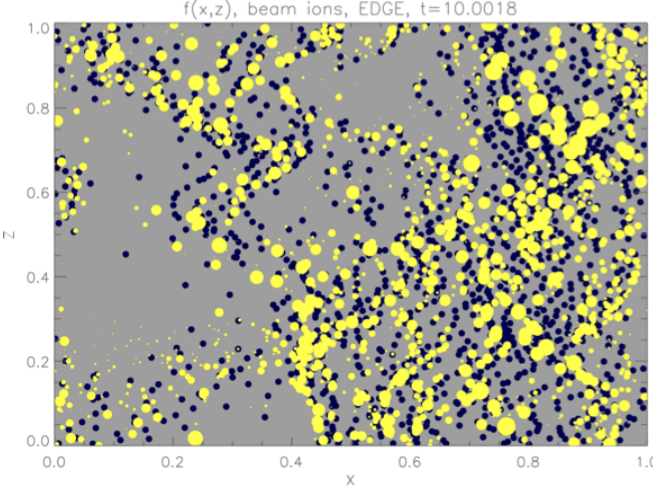


FIG. 17. Phase subspace $\{x, z, \text{Log}_{10}(w)\}$, for illustrative purposes. Yellow dots are late generation particles, size shows weight, while blue particles show concurrent reference run. Minor discrepancies in the local number density is due to a 1/100 stridden sampling — and, to some degree, the collapse of phase space from 6D to 2D. This plot can be compared directly with Figures 18 and 16

IV. DISCUSSION & CONCLUDING REMARKS

It is important to realize that our k-means compression and inflation of CMP data in PIC codes is a *global* method, which ‘feels’ all modes present in the volume at hand. Thus, the method will preserve all modes increasingly well for decreasing wavenumbers considered. This contrasts the local methods, mentioned during the Introduction, which effort the conservation of the physics *locally*, rather. We briefly discuss here some obvious limitations of the k-means scheme. We then discuss how these limitations may not be too severe, considering a range of applications for which a global domain method can be utilized.

Applicability limitations on domain sizes

There is a trade-off between the size of domains on which the method is deployed (here sizable MPI domains) and the speed at which the procedure can be executed.

$V_{\text{kmeans}} \rightarrow V_{\text{cell}}$: In this case, our model approaches the full solution pre-merge/-split. We cannot go to cell sized domains due to the convexity issue, which then becomes either detrimental to conservation of the physics, or becomes nullified due to retainment of the full training vector set in question.

$V_{\text{kmeans}} \rightarrow V_{\text{total}}$: In this case, the edge effects approaches a negligible contribution. We *can* encompass the entire domain; even though super-linear

scaling becomes prohibitive for performance this is only a practical limitation, not a physical one. Also, the compression ratio parameter is relieved of any restrictions imposed by convexity in this limit.

While the latter limit can be remedied by accelerated algorithms or hardware acceleration (see below), the former cannot. We are bound by a lower limit on domain volumes to obtain a reasonable compression factor. The domain volume boundary thickness, W_{bound} must be small compared with the domain interior, along all dimensions. $W_{\text{bound}} \equiv 1\Delta x \ll L_x = 32\Delta x$ (per MPI domain) in our study above. Still, a domain volume granularity leading to $W_{\text{bound}} = 1\Delta x \lesssim L_x \equiv [a \text{ few}] \cdot \Delta x$ should be possible.

Demands for memory

The biggest drawback of the current implementation is memory overhead; worst case, we need simultaneous storage for the codebook, as well as training-to-codebook vector mapping of particle IDs, and count of training vectors-per-codebook vector. The total overhead then becomes $(7[\text{real}] + 7/3[\text{integer}])N_{\text{opt}}$, which should be compared with the normal need for a PIC representation (when not employing merging/splitting) of simply $7[\text{real}]N_{\text{opt}}$ particles: an overhead which doubles the memory need.

Careful implementation and re-use of allocated space can reduce the need for memory, but at present we see no way to remove the need for storage of the full codebook vector data set for the ‘k-means’ scheme. This could improve in the future.

One quite obvious way to remove the problem of overhead in connection with the codebook construction might be to replace the weighted ‘k-means’ step with a weighted ‘k-medoids’ scheme. Training vectors are then taken as codebook centers, thus re-cycling previously allocated memory in an elegant and efficient way. We are currently investigating whether ‘k-medoids’ will also perform adequately with respect to the physics — this is not given *a priori*. It is of similar computational complexity as ‘k-means’.

Acceleration of K-Means clustering

The standard Lloyd’s k-means is too slow, even prohibitively so. We cannot obtain a process which is faster than about $\mathcal{O}(M \times K \times D \times i)$, with D the dimensionality (which is 6 for 3D3V) and i is the number of iterations to convergence. For our test case, the time spent in k-means calculations exceeded the entire simulation time by several factors. An accelerated method is clearly needed. To gain sufficient speed in the computation, we need an approximate factor of 40 in speed-up. This

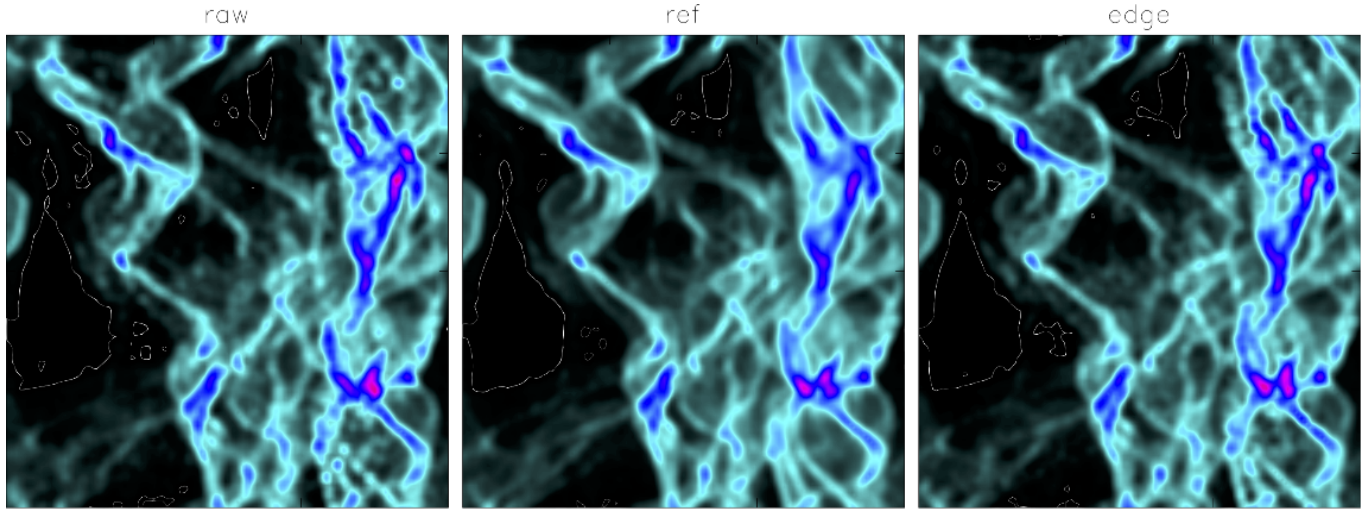


FIG. 18. Comparison between three runs of "Barbara" in the "wide" test case. Contour plots show beam ion density, during automatic merging and splitting on the wide tolerance interval. Approximately 100 merging and 100 splitting events occurred in total on the 16 MPI domains, for an average of about 12 splitting and merging events per domain. We have outlined the lowest level contour (thin white lines) to augment the finest level differences clearly. Number of contour levels is 256, $\max(\rho_{b,i}) \approx 21.0$, $\min(\rho_{b,i}) \approx 0.0$. *Left panel:* raw k-means, no edge filtering. *Middle panel:* reference simulation (no k-means), *Right panel:* edge filtered k-means. The edge-preserving method does perform slightly better, but the differences are very small.

is only possible using more efficient algorithms or more efficient hardware, for the same problem size.

In a separate project, we have investigated acceleration by introducing a KD-Tree method, which seems promising when keeping calculations on CPU. Hardware acceleration is also an option; a GPGPU kernel (in OpenCL) was implemented, with considerable speed-up, on-core. However, the copying of data to-and-fro the GPGPU is costly, and only for large data sets does the hardware accelerated method become feasible. The question of algorithmically accelerated *versus* hardware accelerated k-means will be treated in a subsequent publication (*in preparation*).

For our "BARBARA" test, a typical accelerated k-means step executed about as fast as a typical simulation timestep, making the procedure competitive for several important applications (see Introduction).

With this article we have given an account for a global k-means based phase space compression method, for PIC codes we have assessed the *physical* conservation properties without at glance to *computational* effort. In a forthcoming article (Malý et al.¹⁵) the question of computational cost is addressed in two different ways; by *algorithmic* acceleration (KD-Tree algorithm optimization with MPI+OpenMP support), and by *hardware* acceleration (Lloyd's brute force on GPGPU). Both methods are affirmative towards using our procedure for realistic problems.

Generality of K-Means Merging & Splitting

Particle phase space compression and inflation is not limited to electromagnetic PIC codes. Any system which can be modeled by a discretized particle distribution function, $f(\tilde{\mathbf{r}}(t), t)$, in a D-dimensional space ($\tilde{\mathbf{r}}(t) \in \mathbb{R}^D$) can be manipulated by the k-means optimization scheme described in this article. This means that

1. the number of particles must be high enough to consider the particle population(s) as approximating a continuous distribution within a given volume selected for merging, and
2. that the intrinsic noise in the non-reduced solution must outweigh the noise introduced by the reduction of the particle data set.

The specific values for these constraints are of course problem dependent, the determination of which are beyond the scope of this paper. This question is deferred to future work.

Nonetheless, to give an example here, we have verified the method in one other case of a particle-in-cell based code, by Johansen *et al.*^{7,23} which has shown promising results as well. At a well evolved point in time, in a simulation of the formation of streaming instabilities in a proto-planetary disk, a total of 2.4 million particles were merged into 1.2 million, and the simulation was restarted with the reduced codebook solution. Figure 19 shows a comparison between a reference simulation (black) and the compressed phase space simulation (yellow). The quantity plotted is the (global) maximum CMP number

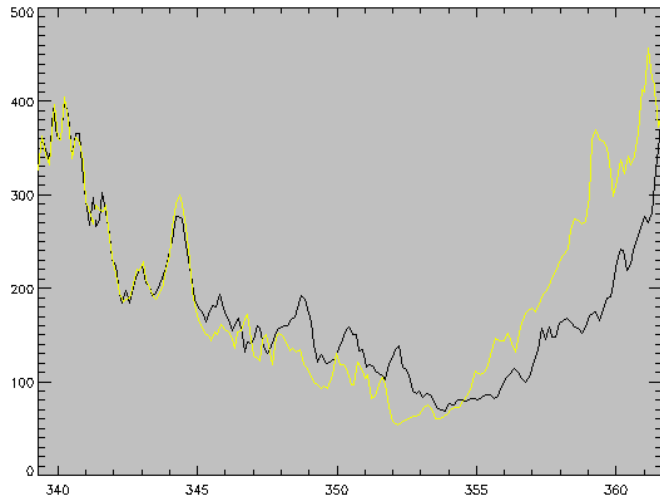


FIG. 19. Global maximum CMP number density, $\max[N_{\text{cell}}(t)]$ in a stand-alone test of the k-means merging procedure on a PIC code used for simulating accretion of planetesimals in planet formation. Black: original particle set (2.4 million CMPs). Blue: reduced set (1.2 million CMPs).

density, $\max[N_{\text{cell}}(t)]$, which is a very sensitive measure. Coherence is almost perfect after 25 iterations and still reasonable after almost 100, even for a reduction by half the particle ensemble. The instance of our k-means algorithm used in this stand-alone test was an early stage implementation, originally employing the Linde-Buzo-Gray algorithm¹², rather than Lloyd-Forgy's. Also, we did not employ our edge-preserving procedure. The agreement plotted here is likely to improve in the future.

Concluding Remark

Without the ability to make a direct comparison by benchmark, it is difficult to assess the range of validity, conservation abilities, computational cost, and possible domain boundary constraints, of the methods mentioned in the Introduction. When we consider the problem from a global PIC domain perspective, the issue of memory overhead associated with performing an analytical match of charge and current densities (without the tensor conservation) could possibly approach that associated with our k-means procedure when $M \lesssim K$. We therefore encourage a comparison of merging methods, in particular between more recent methods^{5,16}, and the statistical k-means based optimization scheme introduced in the present article.

The clustering merge/split code used for this publication may be requested by emailing the author²⁰.

ACKNOWLEDGMENTS

JTF is grateful to Mordechai Butrashvily and Lukáš Malý for their work leading to the software and hardware accelerated versions of k-means (via the 'Summer of PRACE' exchange program, 2013). JTF is thankful for early discussions with Shahab Fatemi, on straightforward subgridding methods, and acknowledges Å. Nordlund and T. Haugbølle, for discussions concerning integration of the k-means framework into the Photon-Plasma code. Research leading to this article was initiated during the EU-FP7 Collaborative Project 'SWIFF' (<http://www.swiff.eu>). Simulations leading to the result presented in Figure 1, were performed¹ using the PRACE Research Infrastructure resource FERMI based in Italy at CINECA. JTF and MEP acknowledge support from the Young Investigator Programme of the Villum Foundation.

- ¹Beck, A. (2015, Apr.). The CILEX-Apollon laser wakefield accelerator configuration experiment. private communication, *work in progress*.
- ²Forgy, E. W. (1965). Cluster analysis of multivariate data : efficiency versus interpretability of classifications. *Biometrics* *21*, 768–769.
- ³Frederiksen, J. T. (2008, June). Stochastically Induced Gamma-Ray Burst Wakefield Processes. *Astrophysical Journal Letters* *680*, L5–L8.
- ⁴Frederiksen, J. T., C. B. Hededal, T. Haugbølle, and Å. Nordlund (2004, June). Magnetic Field Generation in Collisionless Shocks: Pattern Growth and Transport. *Astrophysical Journal Letters* *608*, L13–L16.
- ⁵Grasso, G., M. Frignani, F. Rocchi, and M. Sumini (2010, August). Hierarchical agglomerative sub-clustering technique for particles management in PIC simulations. *Nuclear Instruments and Methods in Physics Research A* *620*, 56–62.
- ⁶Haugbølle, T., J. T. Frederiksen, and Å. Nordlund (2013, June). photon-plasma: A modern high-order particle-in-cell code. *Physics of Plasmas* *20*(6), 062904.
- ⁷Johansen, A. and A. Youdin (2007, June). Protoplanetary Disk Turbulence Driven by the Streaming Instability: Nonlinear Saturation and Particle Concentration. *The Astrophysical Journal* *662*, 627–641.
- ⁸LaKaemper, R. (2004, Sept.). Cis350. <http://knight.temple.edu/~lakamper>.
- ⁹Lapenta, G. (2002, September). Particle Rezoning for Multidimensional Kinetic Particle-In-Cell Simulations. *Journal of Computational Physics* *181*, 317–337.
- ¹⁰Lapenta, G. and J. U. Brackbill (1994, November). Dynamic and Selective Control of the Number of Particles in Kinetic Plasma Simulations. *Journal of Computational Physics* *115*, 213–227.
- ¹¹Lapenta, G. and J. U. Brackbill (1995, May). Control of the number of particles in fluid and MHD particle in cell methods. *Computer Physics Communications* *87*, 139–154.
- ¹²Linde, Y., A. Buzo, and R. Gray (1980, Jan). An algorithm for vector quantizer design. *Communications, IEEE Transactions on* *28*(1), 84–95.
- ¹³Lloyd, S. (1982, Mar). Least squares quantization in pcm. *Information Theory, IEEE Transactions on* *28*(2), 129–137.
- ¹⁴MacQueen, J. (1967). Some methods for classification and analysis of multivariate observations. In *Proc. 5th Berkeley Symp. Math. Stat. Probab., Univ. Calif. 1965/66*, Volume 1, pp. 281–297.
- ¹⁵Malý, L., M. Butrashvily, J. T. Frederiksen, and M. R. B. Kristensen (2015). Accelerated K-Means Clustering for Data Compression. in preparation.

¹⁶Martin, R. S. and J.-L. Cambier (2012, November). Moment preserving adaptive particle weights using octree velocity distributions for PIC simulations. In M. Mareschal and A. Santos (Eds.), *American Institute of Physics Conference Series*, Volume 1501 of *American Institute of Physics Conference Series*, pp. 872–879.

¹⁷Note1. Formally, the original formulation considered only evenly spaced points in one dimension, but the algorithm is not limited to specific point data densities nor one dimension.

¹⁸Note2. Note that this does not imply that the solution physics is only good to 1%, it is much better as can be seen from section on tests.

¹⁹Note3. We do not need an exact solution, only one good enough to subside the Poisson noise in the original CMP ensemble.

²⁰Note4. Proper citation of this article (or co-authorship) should follow application, transcript or re-engineering of the acquired code.

²¹Timokhin, A. N. and J. Arons (2013, February). Current flow and pair creation at low altitude in rotation-powered pulsars' force-free magnetospheres: space charge limited flow. *Monthly Notices of the Royal Astronomical Society* 429, 20–54.

²²Vogelsberger, M. and S. D. M. White (2011, May). Streams and caustics: the fine-grained structure of Λ cold dark matter haloes. *Monthly Notices of the Royal Astronomical Society* 413, 1419–1438.

²³Youdin, A. and A. Johansen (2007, June). Protoplanetary Disk Turbulence Driven by the Streaming Instability: Linear Evolution and Numerical Methods. *The Astrophysical Journal* 662, 613–626.